Supplementary information for

Luminescent Zr(IV) metal-organic frameworks as sensors of waterborne persistent organic pollutants: reproducibility and transferability

Anna Mauri,[a] Gioele Colombo,[a] Simona Galli[a,b,*]

[a] Dipartimento di Scienza e Alta Tecnologia, Università degli Studi dell'Insubria
Via Valleggio 9, 22100 Como, Italy
[*]simona.galli@uninsubria.it
[b] Consorzio Interuniversitario Nazionale per le Scienze e Tecnologie dei Materiali (INSTM),
Via Giusti 7, 50121 Firenze, Italy

Content

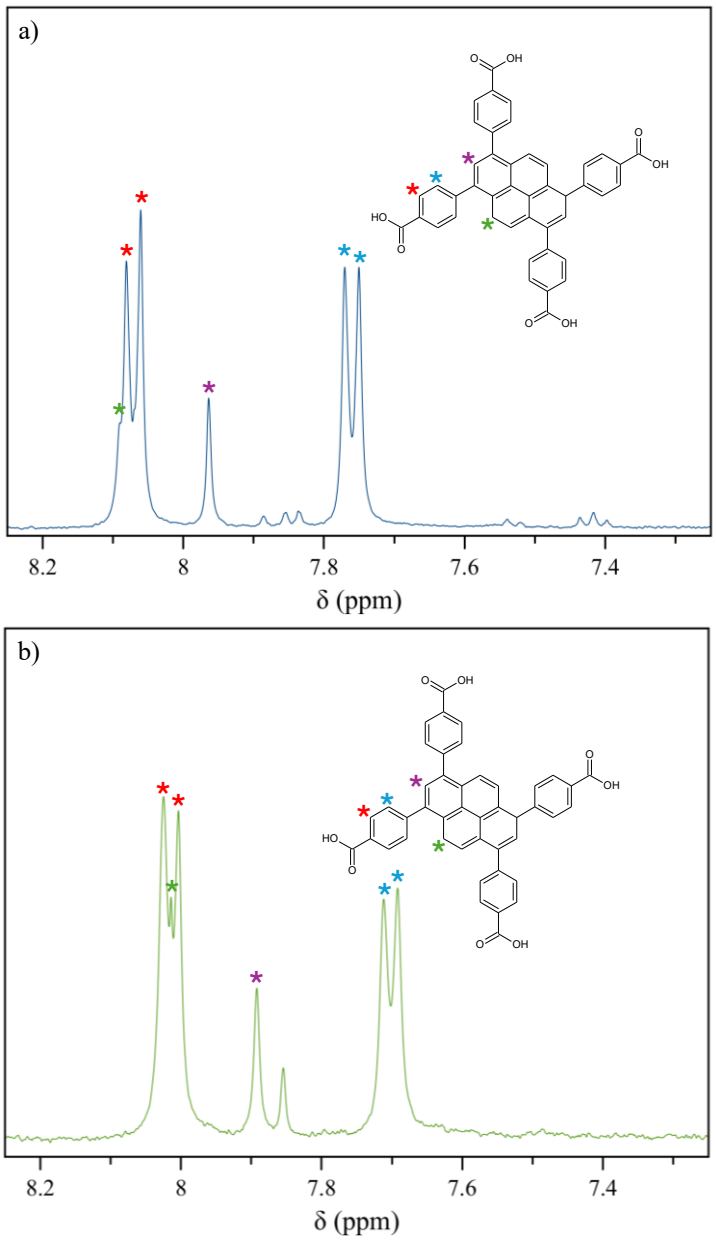

Fig. S1 ^{1}H-NMR spectra acquired in DMSO-d_6 at room temperature on a sample of a) NU-1000 and b) NU-901 after thermal activation followed by digestion in deuterated sulfuric acid.

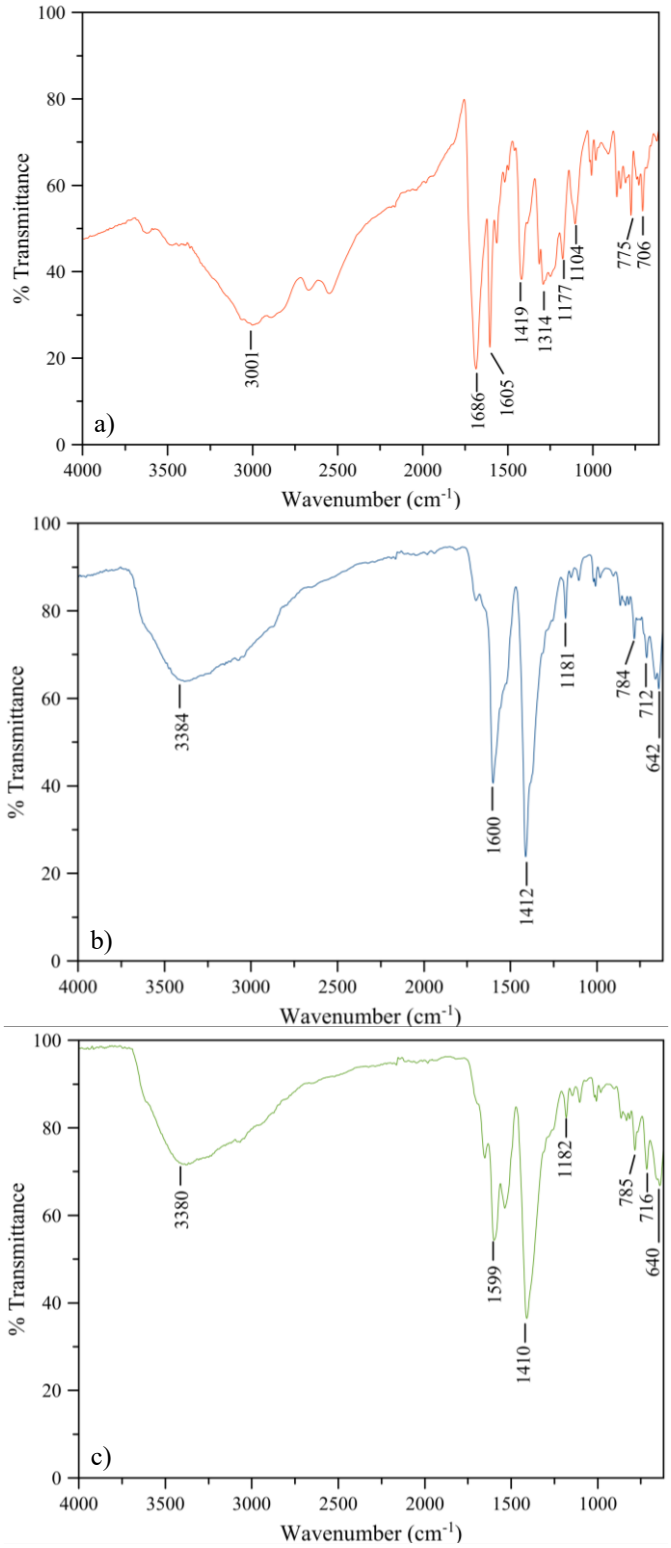

Fig. S2 IR spectra (neat, cm^{-1}) of a) H_4TBAPy [3001, s, vb, ν(OH); 1686, s, sh, ν(C=O); 1314, m, b, ν(C–O)] and thermally activated b) NU-1000 and c) NU-901. For the interpretation of the main bands in the IR spectra of NU-1000 and NU-901 the reader is referred to the Experimental Section of the paper.

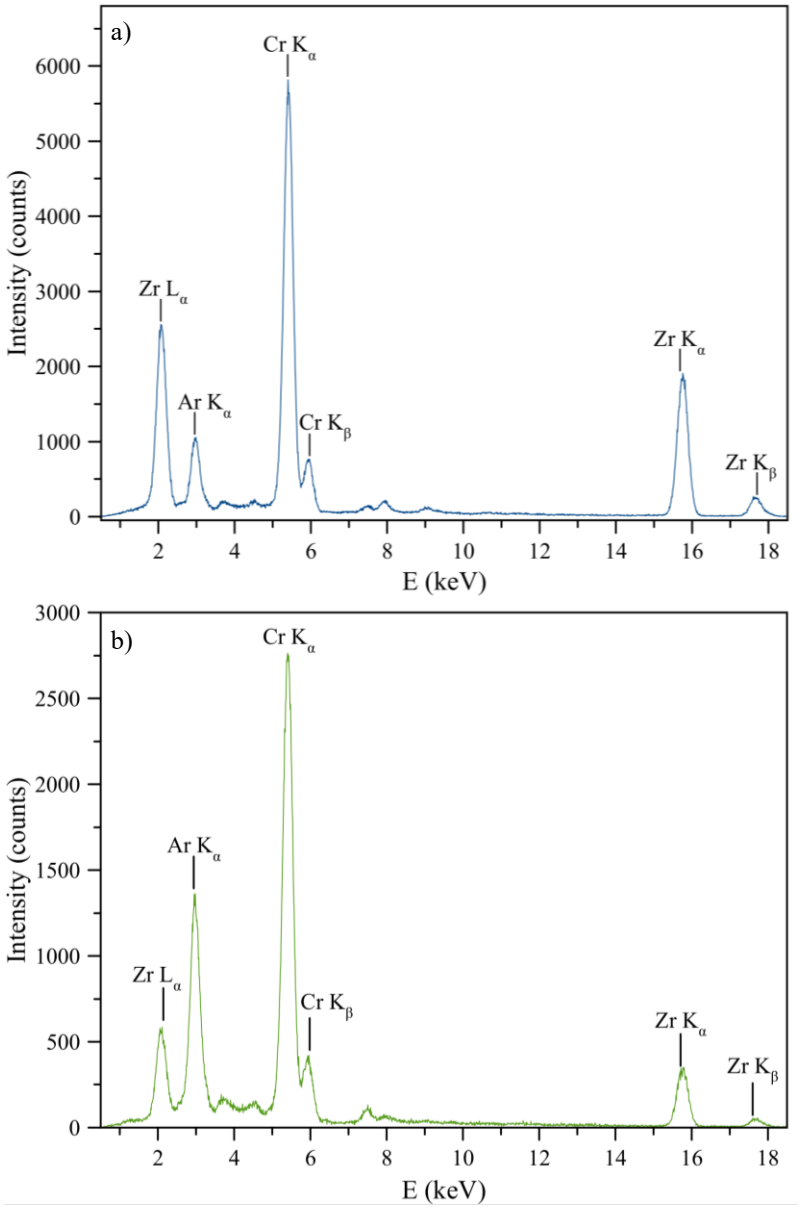

Fig. S3 X-ray fluorescence spectra of thermally activated a) NU-1000 and b) NU-901. The characteristic lines of Cr are due to the composition of the instrument anode, as quoted in the Experimental Section of the paper, while the characteristic line of Ar derives from the fact that the spectra were acquired in air.

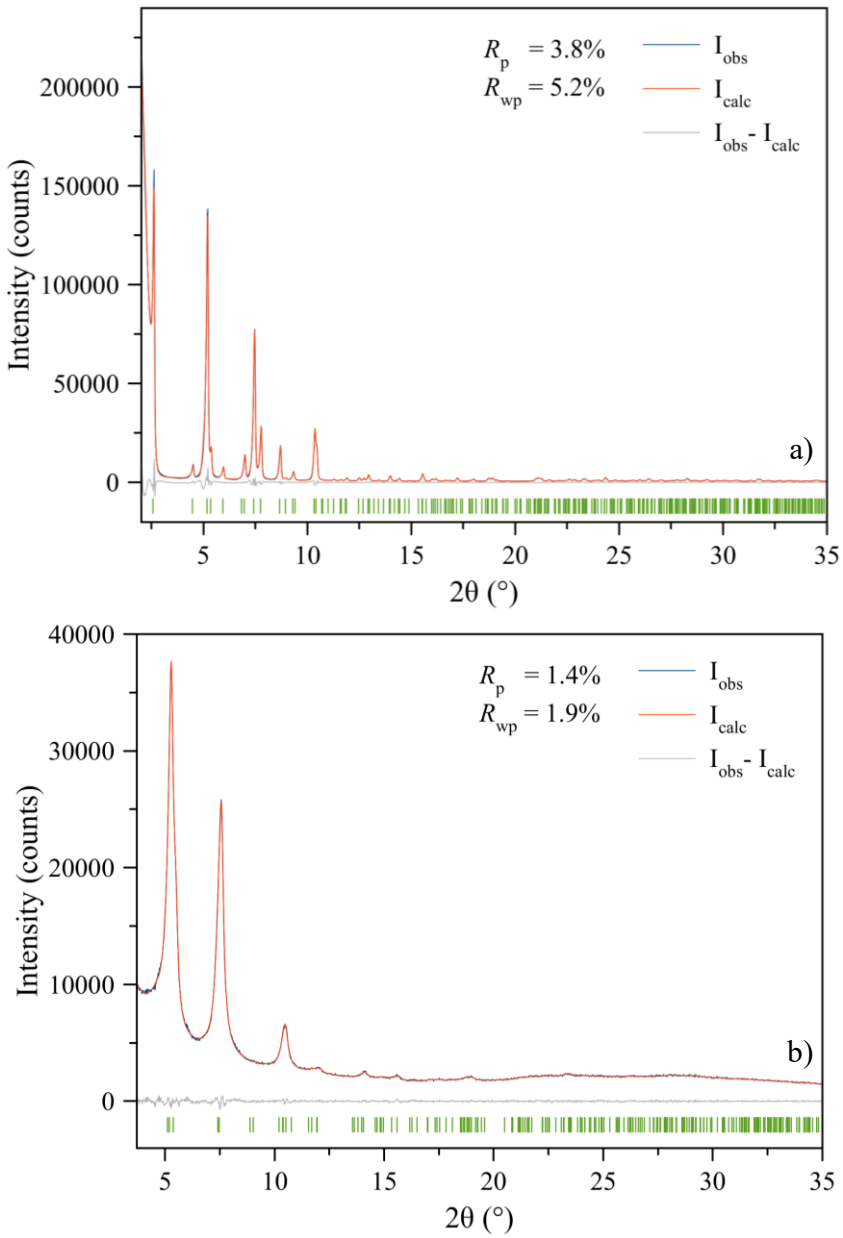

Fig. S4 Graphical result of the last step of the whole powder pattern refinement carried out with the Le Bail approach on the PXRD patterns of thermally activated a) NU-1000 and b) NU-901, starting from the reported crystallographic information (1 and 2 for NU-1000 and NU-901, respectively). Experimental, calculated, and difference patterns: blue, red, and gray traces, respectively. The ticks above the horizontal axis indicate the Bragg reflection maximum positions.

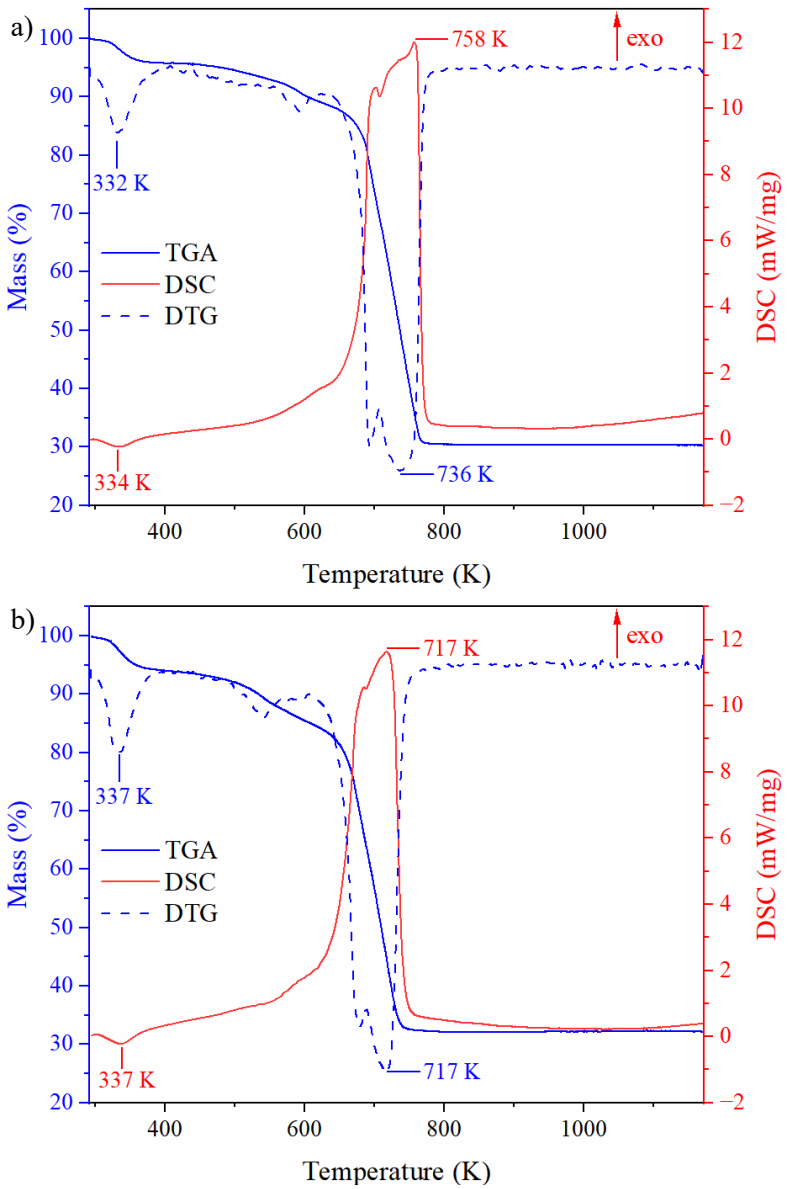

Fig. S5 TG (solid blue line), DTG (dashed blue line) and DSC (orange line) curves of thermally activated a) NU-1000 and b) NU-901 acquired simultaneously under a flow of synthetic air.

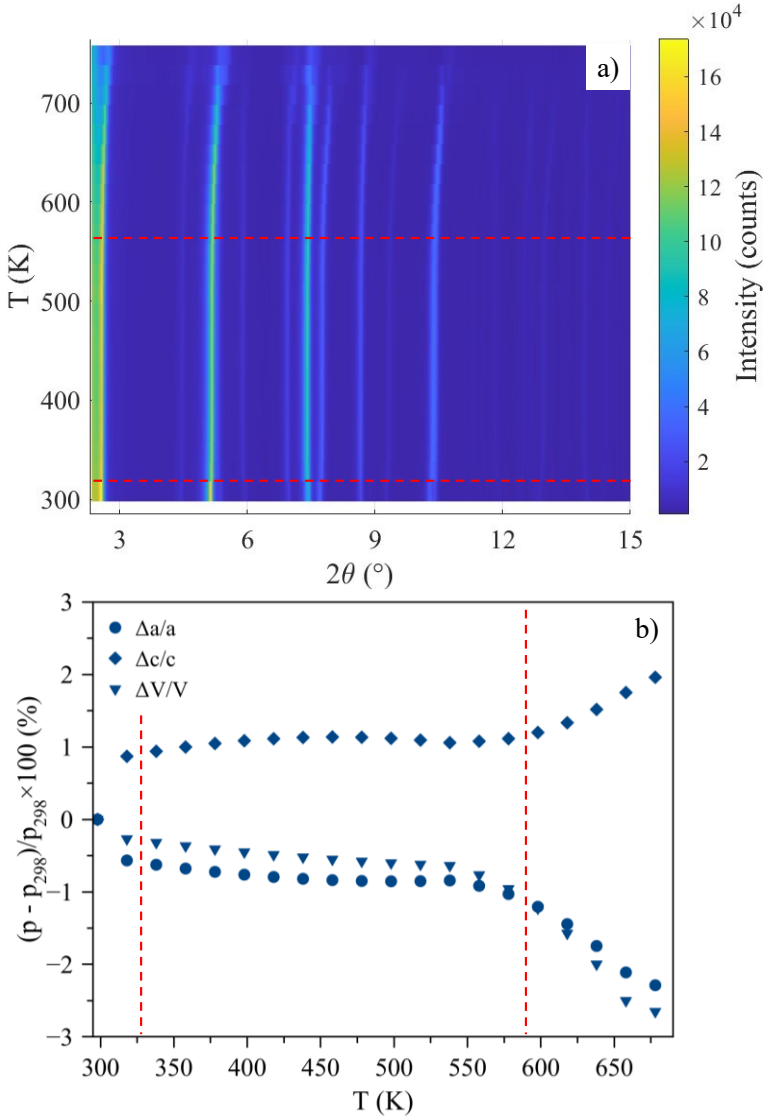

Fig. S6 a) TR-PXRD patterns acquired in air on a sample of thermally activated NU-1000 in the 298-758 K range. b) Percentage relative variation of the unit cell parameters of NU-1000 retrieved through a parametric whole powder pattern refinement performed with the Le Bail method on the 298-658 K TR-PXRD patterns shown in a). The red dashed lines indicate the temperature values at which the unit cell parameters undergo an abrupt variation. More in detail: over the 298-658 K temperature range, the crystallographic *a*-axis and *c*-axis decreases and increases, respectively. This occurrence results in an overall shrinkage of the unit cell volume. Upon passing from 298 to 318 K, the unit cell axes and volume undergo the first abrupt modification ($\Delta a/a_{298}$ = -0.6%; $\Delta c/c_{298}$ = 0.9%; $\Delta V/V_{298}$ = -0.3%) due to the beginning of water loss, as highlighted by simultaneous thermal analysis (see Section 3.3 in the paper and **Fig. S5a**). Then, up to *ca.* 550 K, the three unit cell parameters vary at a slower pace. The variation rate increases again at higher temperatures (for the 298-558 and 298-678 K ranges, respectively: $\Delta a/a_{298}$ = -0.9% and -2.3%; $\Delta c/c_{298}$ = 1.1% and 2.0%; $\Delta V/V_{298}$ = -0.8% and -2.7%).

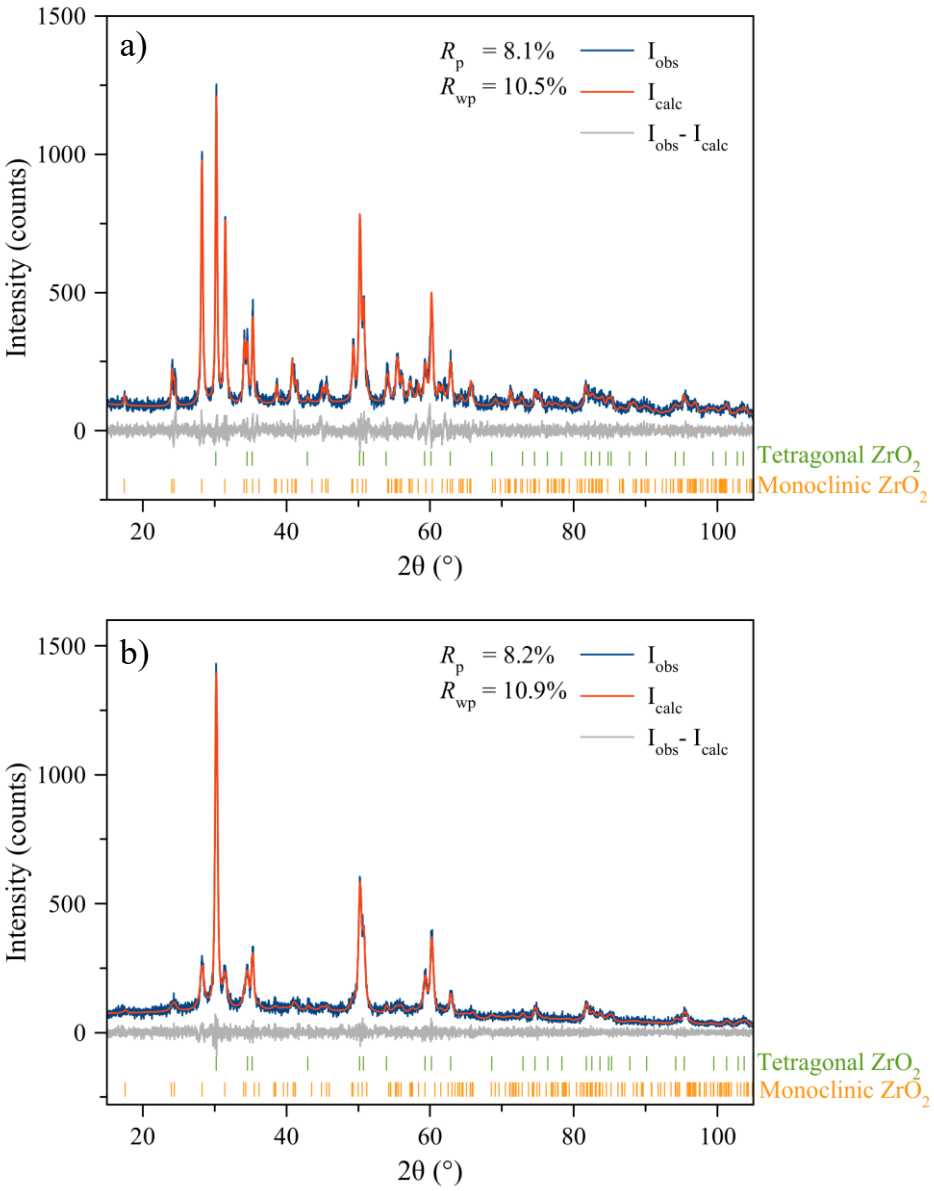

Fig. S7 Final stage of the whole powder pattern refinement performed with the Le Bail approach on the PXRD pattern of the residues recovered after the simultaneous thermal analysis performed on thermally activated a) NU-1000 and b) NU-901 (see **Fig. S5** for the relevant thermograms).

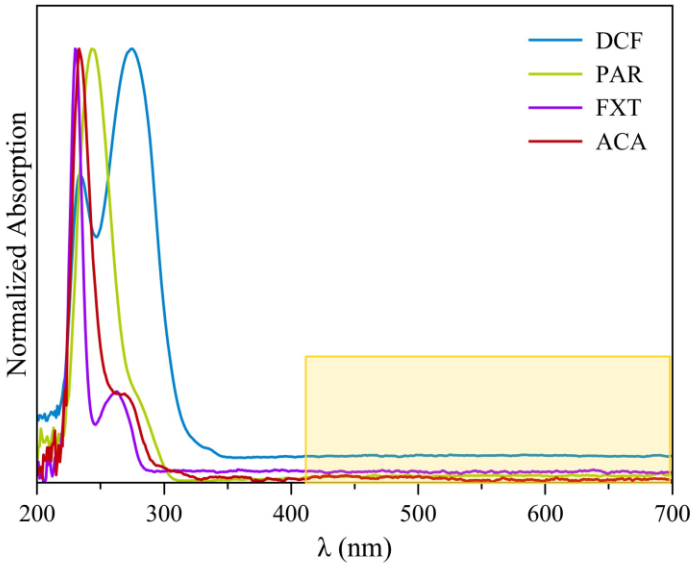

Fig. S8 Normalized UV-Vis electronic absorption spectra of 50 μM aqueous solutions of the selected POPs [diclofenac sodium (DCF), fluoxetine hydrochloride (FXT), paracetamol (PAR) and acetylsalicylic acid (ACA); Scheme 1 in the paper]. Highlighted with a yellow rectangle, the spectral region investigated during the sensing tests (namely: 411-700 nm and 445-700 nm for NU-1000 and NU-901, respectively).

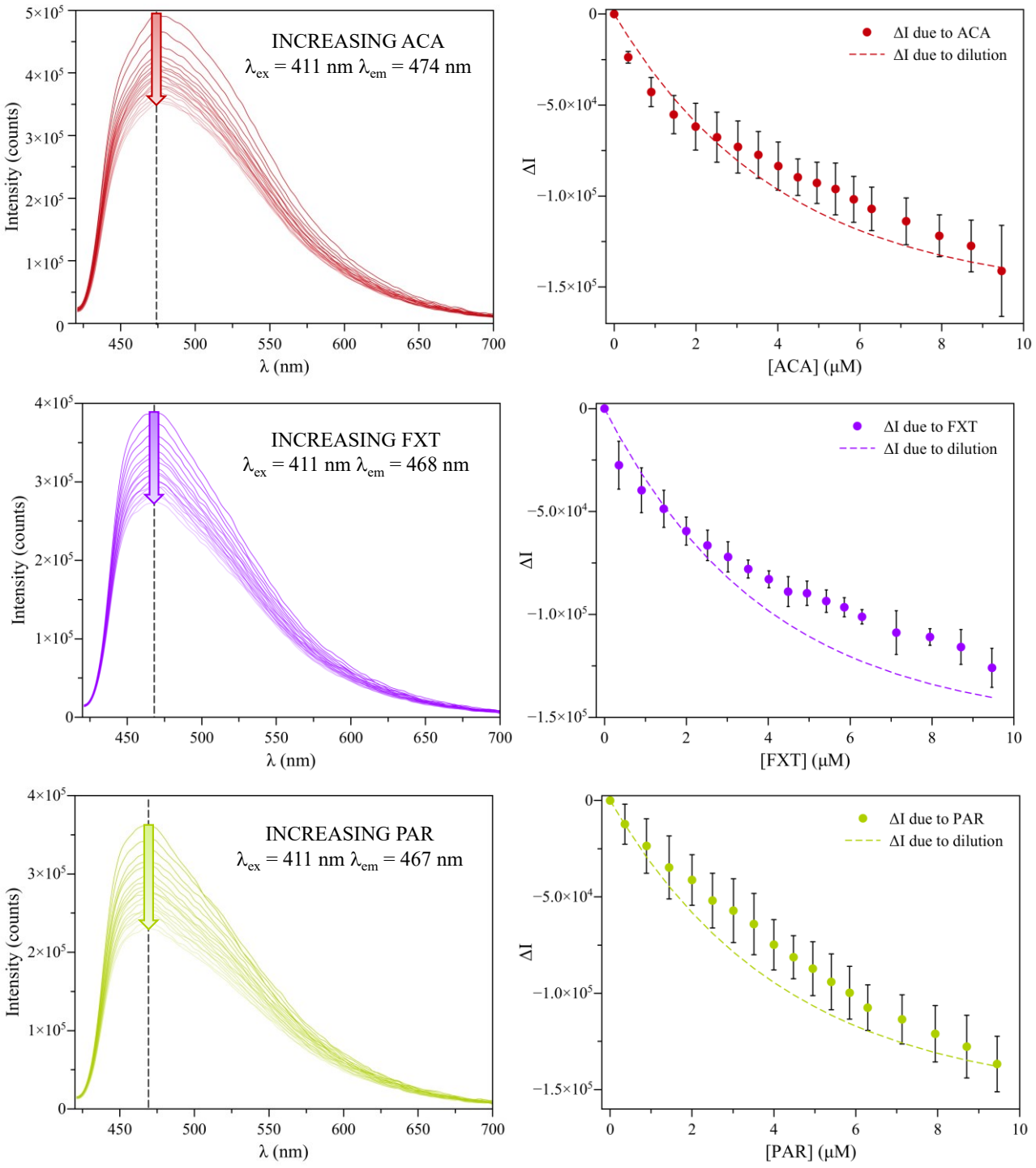

Fig. S9 Left: fluorescence emission spectra of NU-1000 suspended in POP distilled water solutions of increasing concentration (from top to bottom: ACA, FXT and PAR). Right: emission intensity variation ($\Delta I = I_x - I_0$, where I_x and I_0 are the maximum intensity at a given POP concentration and at the zero-point, respectively), averaged over three replicates, as a function of POP concentration (from top to bottom: ACA, FXT and PAR). The dashed curve models the intensity variation due to dilution (see Sections 2.6 and 3.4 of the paper). The vertical bars represent the standard deviation of the three replicates.

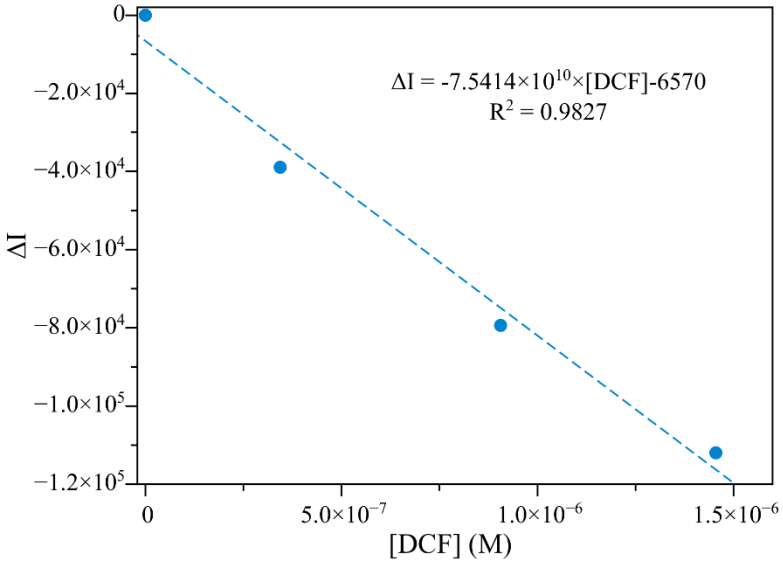

Fig. S10 NU-1000 emission intensity variation as a function of DCF concentration in distilled water solutions 0-1.45 μM, where a linear fitting was performed (dashed line; relevant equation as inset) and was used for the calculation of the limit of detection.

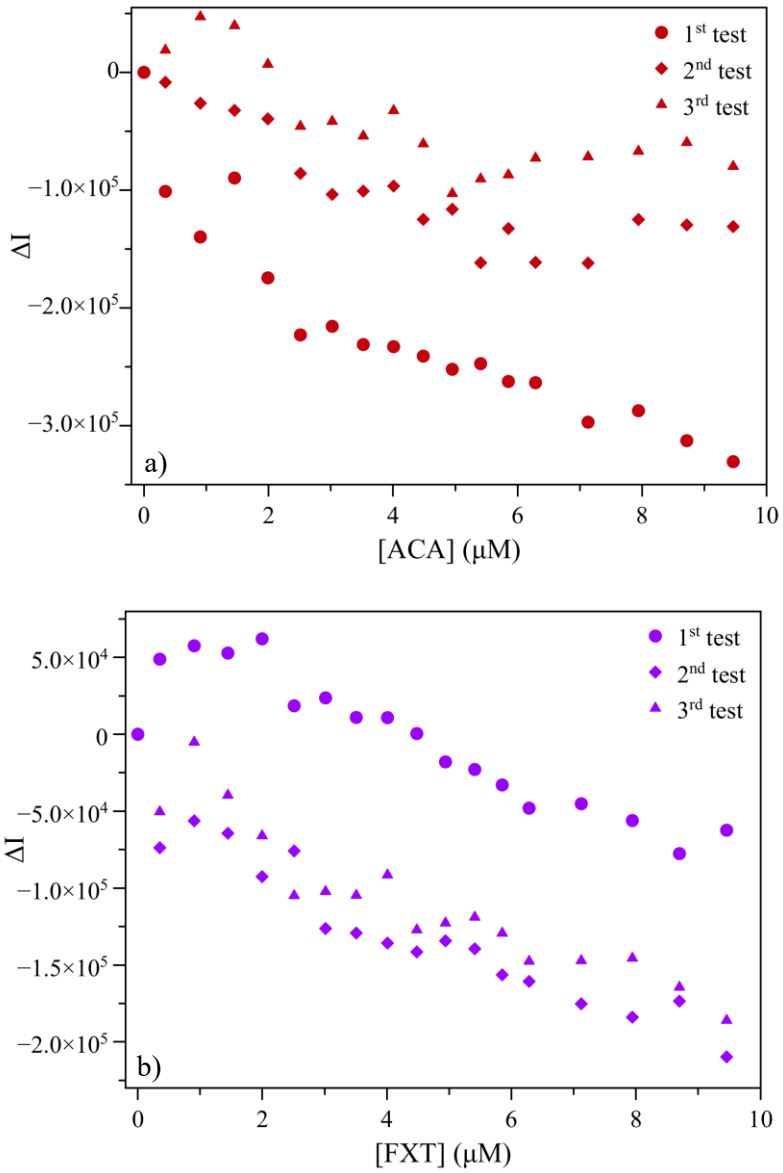

Fig. S11 NU-901 emission intensity variation as a function of the concentration of a) ACA and b) FXT distilled water solutions across three replicates.

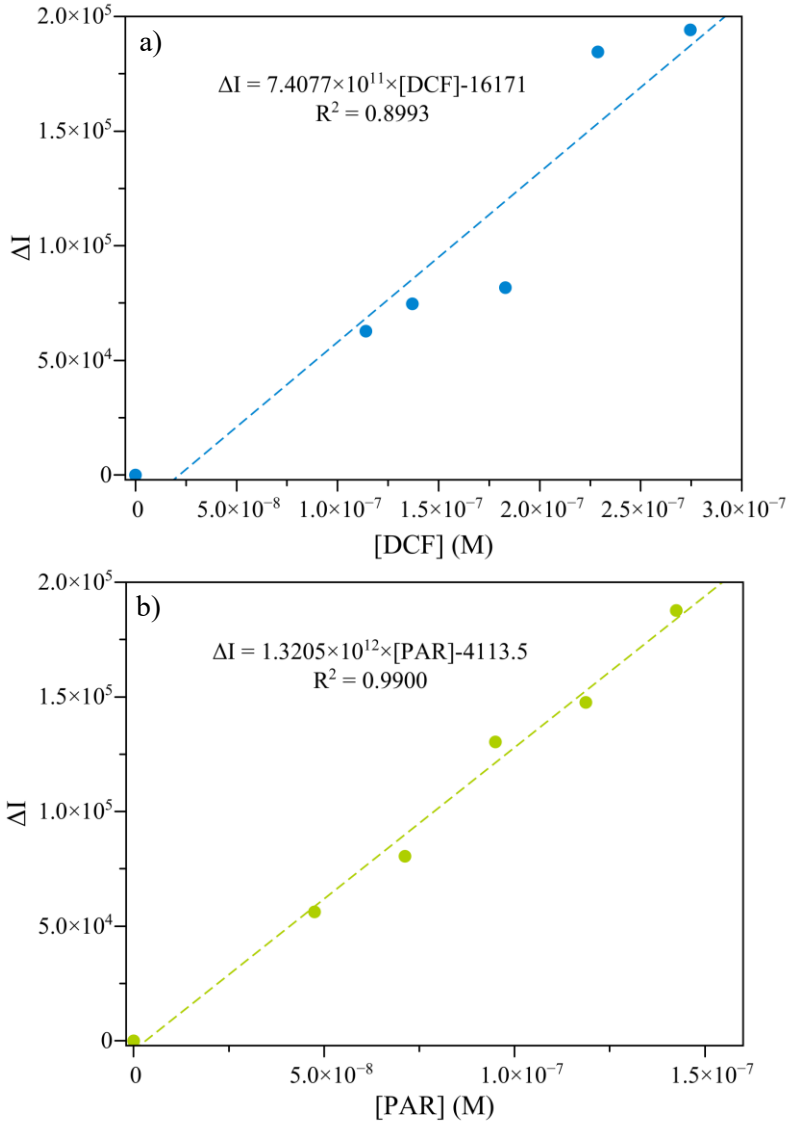

Fig. S12 NU-901 emission intensity variation as a function of the concentration of a) DCF in distilled water solutions 0-2.7×10^{-1} μM and b) PAR in distilled water solutions 0-1.4×10^{-1} μM. Linear fittings were performed (dashed lines; relevant equations as inset) and were used for the calculation of the limit of detection.

Table S1 Volume of POP stock solution (molar concentration reported in the first row) added to the cuvette containing the MOF suspension. For each added volume, the corresponding POP concentration in the cuvette is reported.

DCF (0.046 mM)		FXT (0.047 mM)		PAR (0.048 mM)		ACA (0.046 mM)	
V_{add} (µL)	[DCF] (µM)	V_{add} (µL)	[FXT] (µM)	V_{add} (µL)	[PAR] (µM)	V_{add} (µL)	[ACA] (µM)
15	0.34	15	0.35	15	0.36	15	0.34
40	0.91	39	0.91	38	0.89	40	0.91
65	1.45	63	1.45	62	1.44	65	1.45
90	1.99	88	2.00	87	2.00	90	1.99
115	2.51	112	2.51	110	2.50	115	2.51
140	3.02	136	3.02	134	3.01	140	3.02
165	3.52	160	3.51	158	3.51	165	3.52
190	4.01	185	4.01	182	4.00	190	4.01
215	4.49	209	4.48	206	4.48	215	4.49
240	4.95	233	4.95	230	4.95	240	4.95
265	5.41	258	5.42	254	5.40	265	5.41
290	5.85	282	5.86	278	5.85	290	5.85
315	6.29	306	6.29	302	6.29	315	6.29
365	7.13	354	7.13	349	7.13	365	7.13
415	7.94	403	7.95	397	7.94	415	7.94
465	8.72	450	8.71	444	8.71	465	8.72
515	9.46	499	9.46	491	9.46	515	9.46

Table S2 Chemical analysis, performed by the Department of Chemical Sciences of the University of Naples in 2022, reported by the vendor of the sample of bottled water used in the present study.

Dissolved species	Concentration (mg/L)
Bicarbonate	300
Calcium	49.8
Magnesium	28.5
Nitrate	9
Sodium	5.9
Sulphate	4.9
Chloride	3.0
Potassium	0.99
Fluoride	<0.1
pH at the spring temperature (16 °C) = 7.6	
Electrical conductivity at 20 °C = 420 μS/cm	
Dry residue (180 °C) = 273 mg/L	
Free CO_2 < 10 mg/L	
Silica = 16.5 mg/L	

Table S3 Chemical analysis of municipal tap water as reported on July 2025 (sampling period of the present work) by the company managing the municipal supply (Como Acqua S.r.l.).

Dissolved species	Concentration (mg/L)
Ammonium	<0.02
Calcium	55
Magnesium	13
Nitrate	12
Sodium	<15
Sulphate	14
Chloride	7
Potassium	<5
Fluoride	<0.20
pH at 20 °C = 7.8	
Electrical conductivity at 20 °C = 371 μS/cm	
Dry residue (180 °C) = 230 mg/L	
Hardness = 19 °F	

Table S4 Salient results of the whole powder pattern refinements performed with the Le Bail method on the PXRD patterns of a sample of NU-1000 prior to and after suspension in distilled water for different time lapses *t*.

t (h)	*a* (Å)	*c* (Å)	*V* (Å^3)	Crystal size[a] (nm)	Data, parameters	R_p, R_{wp} (%)
0	39.505(3)	16.542(2)	22358(4)	237(7)	1650, 18	3.7, 5.4
2	39.473(6)	16.586(3)	22381(8)	145(5)	1650, 18	3.5, 4.9
4	39.427(6)	16.585(3)	22328(8)	119(4)	1650, 18	3.0, 4.3
6	39.430(8)	16.595(4)	22344(11)	98(2)	1650, 17	3.3, 4.5

[a] Average crystal size domain assuming a spherical morphology.

Table S5 Salient results of the whole powder pattern refinements performed with the Le Bail method on the PXRD patterns of a sample of NU-901 prior to and after suspension in distilled water for different time lapses *t*.

t (h)	*a* (Å)	*b* (Å)	*c* (Å)	*V* (Å^3)	Crystal size[a] (nm)	Data, parameters	R_p, R_{wp} (%)
0	34.70(2)	18.49(1)	16.84(1)	10803(12)	33.7(3)	1500, 15	2.4, 3.1
2	34.83(2)	18.42(2)	16.94(1)	10873(14)	31.5(4)	1500, 15	2.4, 3.1
4	34.77(2)	18.35(1)	16.88(1)	10766(13)	32.7(4)	1500, 15	2.5, 3.2
6	34.87(2)	18.38(1)	16.940(9)	10857(10)	34.3(3)	1500, 15	2.5, 3.3

[a] Average crystal size domain assuming a spherical morphology.

Table S6 NU-1000 emission intensity maxima ($\lambda_{fluo,max}$) observed at room temperature in experimental condition similar to those of the present work.

$\lambda_{fluo,max}$ (nm)	Solvent	λ_{ex} (nm)	Reference
463-501[a]	Water	411	This work
450	Water	385	[3]
518	Water	418	[4]
491	Methanol	310	[5]
440	NEM buffer[b]	385	[6]
500	Water	360	[7]
480	Water	340	[8]
465	Water	395	[9]

[a] See Section 3.4 of the paper for further details. [b] NEM = N-ethylmorpholine.

Table S7 UV-Vis electronic absorption maxima ($\lambda_{abs,max}$) of diclofenac sodium (DCF), fluoxetine hydrochloride (FXT), paracetamol (PAR) and acetylsalicylic acid (ACA), as observed in the present work and previously reported in the literature.

	$\lambda_{abs,max}$ (nm)	
POP	This work	Previous works[10]
DCF	234, 274	275.5
PAR	244	243
FXT	230, 262	230
ACA	233, 269	225, 274

Table S8 Top panel: NU-1000 average emission intensity variation observed in 6.3 μM distilled water solutions of DCF, FXT, PAR and ACA as input for the Tukey's HSD test. Bottom panel: results of the test (q_{crit} = 4.53 for 4 groups and 8 degrees of freedom, α = 0.05).

DCF	FXT	ACA	PAR
-248189	-102263	-119995	-94308
-267311	-104006	-104609	-117167
-264679	-97221	-96634	-110949

POP1	POP2	q-cal
DCF	PAR	26.41
DCF	FXT	27.50
DCF	ACA	26.50
PAR	FXT	1.10
PAR	ACA	0.07
FXT	ACA	1.02

Table S9: Comparison of DCF limits of detection shown by NU-1000 and NU-901 in the present work with those of other MOFs reported in the literature.

MOF	LoD (M)	Reference
NU-1000	5×10^{-7}	This work
NU-901	3×10^{-7}	This work
Zr_BTDZ[a]	4.1×10^{-6}	[11]
TTz@PCN-700[a]	9×10^{-5}	[12]
TzPhTzMe@PCN-700[a]	8.4×10^{-6}	[12]
FMOF-5	4.1×10^{-6}	[13]

[a] H_2BTDZ = 4,4′-(benzothiadiazole-4,7-diyl)dibenzoic acid; H_2TTZ = thiazolo[5,4-*d*]thiazole-2,5-dicarboxylic acid; H_2TzPhTzMe = 2,2′-(1,4-phenylene)bis(4-methylthiazole-5-carboxylic acid).

References

1 J.E. Mondloch, W. Bury, D. Fairen-Jimenez, S. Kwon, E.J. DeMarco, M.H. Weston, A.A. Sarjeant, S.T. Nguyen, P.C. Stair, R.Q. Snurr, O.K. Farha and J.T. Hupp, *J. Am. Chem. Soc.* 2013, **135**, 10294−10297.

2 L. Robison, R.J. Drout, L.R. Redfern, F.A. Son, M.C. Wasson, S. Goswami, Z. Chen, A. Olszewski, K.B. Idrees, T. Islamoglu and O.K. Farha, *Chem. Mater.* 2020, **32**, 3545−3552.

3 L. Luconi, G. Mercuri, T. Islamoglu, A. Fermi, G. Bergamini, G. Giambastiani and A. Rossin, *J. Mater. Chem. C* 2020, **8**, 7492-7500.

4 Z.-J. Lin, H.-Q. Zheng, H.-Y. Zheng, L.-P. Lin, Q. Xin and R. Cao, *Inorg. Chem.* 2017, **56**, 14178−14188.

5 W. Hao, G. Huang, G Jiang, S.A. Dauda and F. Pi, *Food Bioscience* 2023, **55**, 102967-102975.

6 F. Gabriel, A. Roussey, S.S. Nobre and A. Carella, *J. Mater. Chem. C* 2024, **12**, 11378-11385.

7 Y. Zhou, Q. Yang, J. Cuan, Y. Wang, N. Gan, Y. Cao and T. Li, *Analyst* 2018, **143**, 3628-3634.

8 J. Han, Y. Miao, J. Cuan, H. Zhou, S. Zhu, Z. Wu and Y. Zhou, *Anal. Chem.* 2023, **95**, 6612−6619.

9 D. Ning, Q. Liu, Q. Wang, X.-M. Du, Y. Li and W.-J. Ruan, *Dalton Trans.* 2019, **48**, 5705-5712.

10 DCF: D.R. Lima, A.A. Gomes, E.C. Lima, C.S. Umpierres, P.S. Thue, J.C.P. Panzenhagen, G.L. Dotto, G.A. El-Changhaby and W.S. de Alencar, *Spectrochim. Acta A* 2019, **218**, 366–373. PAR: T. Bouarroudj, L. Aoudjit, I. Nessaibia, D. Zioui, Y. Messai, A. Bendjama, S. Mezrag, M. Chabbi and K. Bachari, *Russ. J. Phys. Chem.* 2023, **97**, 1074-1087. FXT: M.W. Lam, C.J. Young and S.A. Mabury, *Environ. Sci. Technol*. 2005, **39**, 513-522. ACA: M. Nayak, C.B. Patel, A. Mishra, R. Singh and R.K. Singh, *J. Fluoresc.* 2024, **34**, 1441-1451.

11 G. Provinciali, G. Bicchierai, A.L. Capodilupo, A. Mauri, J. Fu, D. Liu, G. Giambastiani, G. Tuci, S. Galli, C. Piccirillo, A. Rossin, *J. Mater. Chem C* 2025, **13**, 16427-16439.

12 G. Provinciali, A.L. Capodilupo, A. Mauri, S. Galli, L. Donà, B. Civalleri, G. Tuci, G. Giambastiani, C. Piccirillo, A. Rossin, *ACS EST Water* 2024, **4**, 2339-2351.

13 H.A. Qader, S.S.M. Ameen, I.B. Qader, K.M. Omer, *Spectrochim. Acta A* 2024, **322**, 124791-124796.